Unique anticodon loop conformation with the flipped-out wobble nucleotide in the crystal structure of unbound tRNA^Val

HYEONJU JEONG and JUNGWOOK KIM

Department of Chemistry, Gwangju Institute of Science and Technology, Gwangju 61005, Korea

ABSTRACT

During protein synthesis on ribosome, tRNA recognizes its cognate codon of mRNA through base-pairing with the anticodon. The 5′-end nucleotide of the anticodon is capable of wobble base-pairing, offering a molecular basis for codon degeneracy. The wobble nucleotide is often targeted for post-transcriptional modification, which affects the specificity and fidelity of the decoding process. Flipping-out of a wobble nucleotide in the anticodon loop has been proposed to be necessary for modifying enzymes to access the target nucleotide, which has been captured in selective structures of protein-bound complexes. Meanwhile, all other structures of free or ribosome-bound tRNA display anticodon bases arranged in stacked conformation. We report the X-ray crystal structure of unbound tRNA^Val1 to a 2.04 Å resolution showing two different conformational states of wobble uridine in the anticodon loop, one stacked on the neighboring base and the other swiveled out toward solvent. In addition, the structure reveals a rare magnesium ion coordination to the nitrogen atom of a nucleobase, which has been sampled very rarely among known structures of nucleic acids.

Keywords: tRNA; crystal structure; wobble nucleotide; base flipping

INTRODUCTION

The primary role of tRNA is to serve as an adaptor in translation, which recognizes a cognate codon on mRNA through base-pairing with the anticodon in the decoding site and brings the matching amino acid conjugated at its 3′-end to the peptidyltransfer site in the small and large subunits of ribosome, respectively. In addition, tRNA is known to be involved in other biologically important processes including bacterial cell wall synthesis, where aminoacyl-tRNA acts as an amino acid donor (Lennarz et al. 1966; Fonvielle et al. 2009; Roy and Ibba 2009), regulation of gene expression with T-box riboswitch in amino acid synthesis (Zhang and Ferré-D'Amaré 2015; Li et al. 2019), and cytochrome c-dependent apoptosis (Mei et al. 2010). Recently, novel regulatory roles of tRNA fragments have emerged in numerous stress response pathways, where tRNA is sensitive to cleavage by stress-induced endonuclease, which is activated by viral infection (Wang et al. 2013), nutrient depletion (Lee and Collins 2005), and oxidative stress (Thompson et al. 2008). The tRNA-derived fragment modulates stress-induced signal by affecting translation in-hibition and stress-induced granule formation (Thompson and Parker 2009; Emara et al. 2010; Ivanov et al. 2011).

The tertiary structure of tRNA folds into a conserved L-shape, which was demonstrated by X-ray crystal structures of yeast tRNA^Phe (Kim et al. 1974; Robertus et al. 1974). The intramolecular hydrogen bonding interactions between the D and TψC stem–loops contribute to the rigidity of the core domain and to maintaining an overall L-shaped structure of the tRNA molecule. For example, G18-ψ55 and G19•C56 base pairs are invariantly conserved. Another characteristic structural feature of tRNA is the U-turn motif observed in the TψC and anticodon loops, where a reversal of phosphate backbone direction occurs (Quigley and Rich 1976). Two invariant uridine residues, U33 and ψ55, play a crucial role in stabilizing the U-turn of anticodon and TψC loops, respectively. One of the key atomic interactions for the anticodon U-turn is the hydrogen bond between the N3 of U33 and the phosphates of N35 and N36. Additionally, the hydrogen bond between

2′-OH of U33 and the nucleobase of N35 has been proposed to be important (Auffinger and Westhof 2001). The sharp turn in the anticodon loop places the wobble nucleotide (N34) at the apex of the tRNA molecule enabling this residue to assume a less restricted conformation, which is necessary to read the cognate codon through wobble base-pairing (Balasubramanian and Seetharamulu 1983).

The wobble pairing can be further modulated by diverse chemical modifications of N34, where analyses of MODOMICS database reveals that ∼40% of tRNA contain a modified nucleotide at the wobble position (Boccaletto et al. 2018). In general, post-transcriptional modifications at N34 facilitate translational processes on the ribosome including the expansion of codon recognition (Yarian et al. 2002; Begley et al. 2007; Weixlbaumer et al. 2007; Kurata et al. 2008), tRNA binding with ribosome (Salman Ashraf et al. 1999; Ashraf et al. 2000), frameshift control (Urbonavičius et al. 2001), and translocation (Phelps et al. 2004; Ranjan and Rodnina 2017). In the X-ray crystal structures of free- and ribosome-bound tRNA, nucleobases of anticodon triplets are stacked along a helical axis, limiting the availability of N34 for enzyme-dependent alterations. Therefore, modifying enzymes must induce the conformational rearrangement of the anticodon loop to present the to-be modified nucleotide to the enzyme active site. The base-flipping mechanism within the anticodon loop has been supported by cocrystal structures of several tRNA modifying enzymes, including pseudouridine synthase (RluA), tRNA guanine transglycosylase (TGT), tRNA-specific 2-thiouridylase (MnmA), and tRNA-specific adenosine deaminase (TadA) (Xie et al. 2003; Hoang et al. 2006; Losey et al. 2006; Byrne et al. 2015). Similarly, crystal structures of aspartyl- and glutaminyl-tRNA synthetase contain tRNA with destacked anticodon residues in the active site of the protein, which serve as a specificity determinant for correct aminoacylation at the 3′-end of tRNA (Rould et al. 1991; Chang et al. 2012). In these structures, the anticodon loop of tRNA undergoes conformational change upon complexation with a partner protein.

Here we present the X-ray crystal structure of unbound *E. coli* tRNA[Val1] at a resolution of 2.04 Å displaying two different conformational states especially of the anticodon loop; that is, anticodon bases are stacked in one tRNA molecule, whereas the wobble uridine is flipped-out in the other. The structural change of the anticodon loop is mainly limited to the wobble nucleotide with all other bases in the loop remaining stacked unlike certain enzyme-bound tRNA structures, in which a more extensive conformational rearrangement occurs. In addition, the high-resolution data allowed us to assign a total of 10 metal ions over two tRNA molecules. Notably, we identified the magnesium binding site next to the guanosine base of G15, which provides a rare example supporting the coordination between Mg^{2+} and the imine nitrogen of nucleobase.

RESULTS

We initially attempted to produce cocrystals of *E. coli* tRNA[Val1] and *Mycoplasma capricolum* YfiC, a putative tRNA methyltransferase targeting the N6 of A37. However, it was evident that protein was not present after solving the structure. The dimension of the unit cell is not large enough to accommodate an additional protein molecule, where the solvent content of the crystal is 64.46%. Crystallographic statistics are summarized in Table 1.

An overall structure of *E. coli* tRNA[Val1]

The asymmetric unit contains two tRNA molecules, protomers A and B, which make contact with each other through the anticodon loop regions (Fig. 1). The overall L-shaped conformation characteristic of tRNA can be observed for both noncrystallographic symmetry (NCS)-related molecules. Nearly all nucleotide residues could be modeled except for the 3′-terminal residue of chain B, or A76$_B$, due to disorder. When superposed, both protomers exhibit a

TABLE 1. Crystallographyic statistics

	E. coli tRNA[Val1] (UAC)
Data collection	
Space group	P 1 21 1
Cell dimensions	
a, *b*, *c* (Å)	53.54 33.06 131.80
α, *β*, *γ* (°)	98.15
Resolution (Å)	30.00–2.04 (2.09–2.04)
R_{sym} or R_{merge}	0.099 (0.827)
$CC_{1/2}$	0.874 (0.775)
I/σ*I*	4.80 (1.33)
Completeness (%)	97.4 (88.9)
Redundancy	6.4 (5.1)
Refinement	
Resolution (Å)	29.49–2.04
No. reflections	28771
R_{work}/R_{free}	0.204/0.236
No. atoms	
Nucleic acid	3221
Metal ions	10
Water	154
B-factors	
Nucleic acid	39.02
Metal ions	41.07
Water	34.06
R.m.s. deviations	
Bond lengths (Å)	0.0078
Bond angles (°)	1.53

Data set was collected from single crystal. Values in parentheses are for the highest resolution shell.
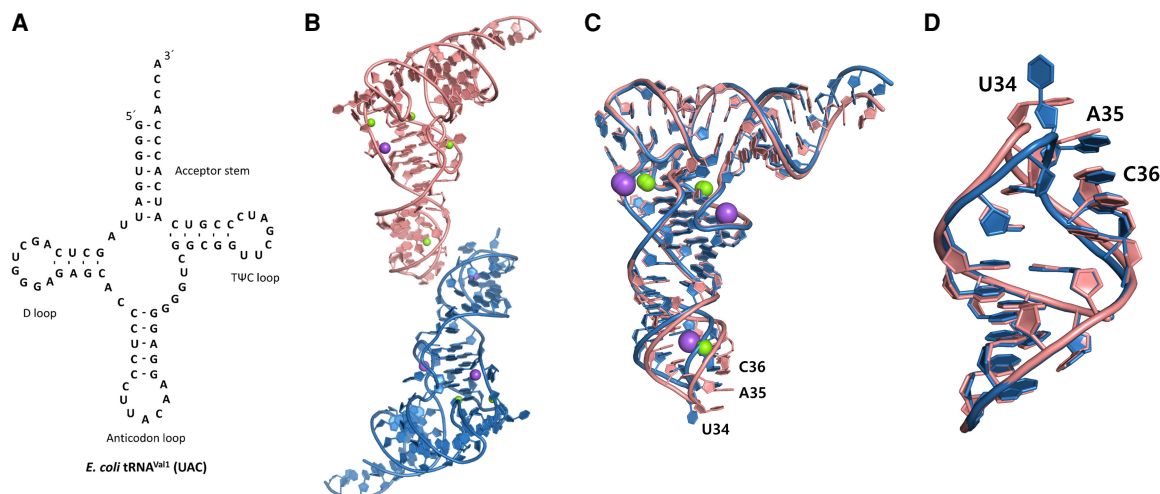
FIGURE 1. The overall structure of *E. coli* tRNA^{Val1} (*A*) Cloverleaf secondary structure of *E. coli* tRNA^{Val1}, which was utilized in the present X-ray crystallographic study. (*B*) A ribbon representation of two NCS-related tRNA^{Val1} molecules in the asymmetric unit cell, where protomer A is shown in blue and protomer B is in salmon. Mg^{2+} and Na$^+$ are displayed in green and purple spheres, respectively. (*C*) Superposition of protomers A and B and identical color scheme is used as in *B*. (*D*) Close-up view of ASL domains from overlaid structures in *C*.

highly similar conformation with an rmsd of 1.94 Å, which align best around the central region mainly composed of D and TψC stem–loops while the greatest deviation is observed in the 3′-termini and anticodon loops. For example, the distances between phosphorous atoms of U34$_A$–U34$_B$ and C75$_A$–C75$_B$ are 7.59 and 6.06 Å, respectively. The present structure contains three base triplets in each protomer; U12•A23–A9, G45–G10•C25, and C13•G22–G46 (Supplemental Fig. 1). Of note, U8 and A14 form the reverse Hoogsteen base pair and the 2′-OH of U8 is within a hydrogen bonding distance from the N1 of A21. Additionally, three tertiary base pairs between D and TψC stem–loops were identified; G15•C48, G18–U55, and A26–G44 (Supplemental Fig. 2).

Distinct conformation of the anticodon loop adopted by tRNA^{Val1}

The hydrogen bond between the N3 of U33 and the OP2 of C36 in the anticodon loops of both protomers is a characteristic structural element of the U-turn motif of tRNA. Additional hydrogen bonds involving U33 stabilize the sharp turn around U34, although detailed interactions are slightly different between two NCS-related molecules as follows: The N3 of U33$_A$ and the OP2 of A35$_A$ and C36$_A$ are within a hydrogen bond distance. In addition, U33$_A$ contacts the N6 of A37$_A$ through two hydrogen bonds, using the O2 of uracil base and the 2′-OH of ribose (Fig. 2A). On the other hand, although the hydrogen bond between the N3 of U33$_B$ and the OP2 of C36$_B$ is conserved, the N1 of U33$_B$ is engaged in electrostatic interaction with the OP2 of A35$_B$ (Fig. 2B). Moreover, U33$_B$ is connected to C36$_B$ via a single hydrogen bond between the 2′-OH of ura-

cil and the N4 of cytidine. The interaction between the 2′-OH of U33 and the base at position 35 has been suggested to be required for the tertiary structure of the anticodon loop U-turn (Auffinger and Westhof 2001). In that regard, the hydrogen bonding mode of the 2′-hydroxyl group of U33 in the present crystal structure is atypical, where the 2′-oxygen atom of U33$_B$ and the N7 of A35$_B$ are 3.79 Å apart from each other. Furthermore, the 2′-OH of U33$_A$ is 10.82 Å away from the N7 of A35$_A$ and interacts with the N6 of A37$_A$ as described above, contributing to the unique conformation of the anticodon loop. The unconventional intramolecular interactions in the anticodon U-turn motif appear to be driven by the dimerization contact between the NCS-related protomers, where A35$_B$ forms three hydrogen bonds with C36$_A$ (Supplemental Fig. 3).
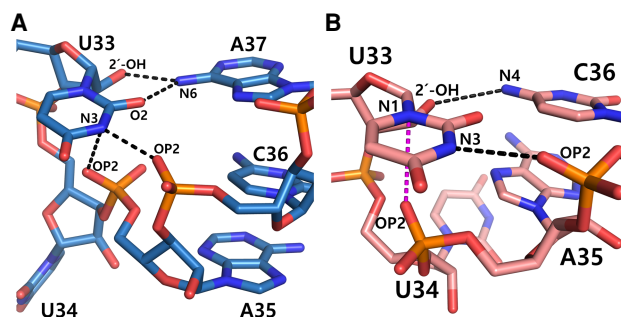
FIGURE 2. Key atomic interactions in the U-turn motif of anticodon loop. Important hydrogen bonding and electrostatic interactions in forming the U-turn within the ASL of protomer A (*A*) and B (*B*) are shown. Hydrogen bonds are depicted in black dashed lines and electrostatic interactions are shown in purple. Note that the N1 of uracil assumes a partial positive charge due to the delocalization of π-electrons.
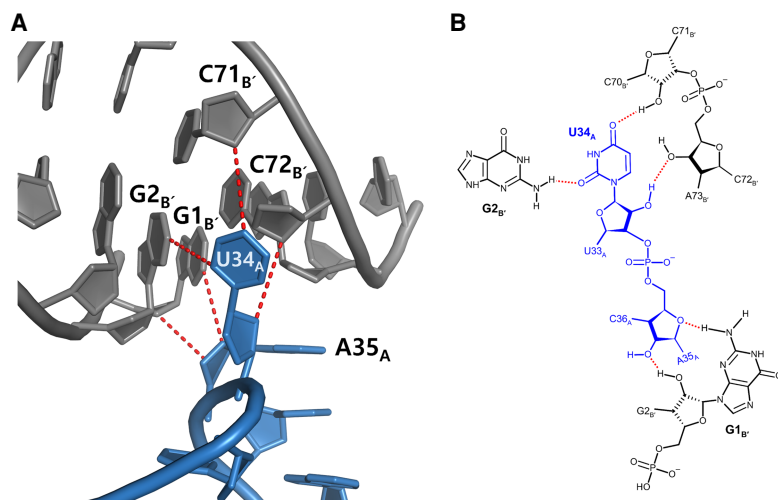
FIGURE 3. The flipped-out wobble uridine. (*A*) The protomer containing the flipped-out U34$_A$ (blue) interacts with the nearby symmetry-related molecule (gray) through hydrogen bonds which are depicted as red dots. Protomer B is not shown for clarity. (*B*) A description of a detailed hydrogen bond interactions at the interface.

The most marked structural difference in the anticodon loop between the two protomers is highlighted in the wobble uridine conformation; whereas U34$_B$ is stacked on G35$_B$, U34$_A$ protrudes out of a helical axis and faces bulk solvent. The flipping-out of U34$_A$ is promoted by the lattice contacts with a nearby symmetry-related molecule, with a buried surface area of 256.4 Å^2 (Fig. 3A). The flipped-out wobble uridine is engaged in three hydrogen bonding interactions with G2$_{B'}$, C71$_{B'}$, and C72$_{B'}$ as shown in Figure 3B. Except for U34$_A$, all other bases on the anticodon loop face the inside and participate in base stacking interactions. Comparison of dihedral angles for each nucleic acid residue on the anticodon stem–loop reveals that the deviation peaks at U33 and U34, especially in $\varepsilon(33)$, $\alpha(34)$, and $\gamma(34)$, which represent the torsion angles around C3′(33)–O3′(33), P(34)–O5′(34), and C5′(34)–C4(34), respectively (Table 2).

Comparison with modified ASL^{Val}

Cellular *E. coli* tRNA^{Val1} contains a total of six post-transcriptional modifications, two of which are located in the anticodon loop; 5-carboxymethoxyluridine (cmo^{5}U34) and N6-methyladenosine (m^{6}A37). Since the present tRNA structure lacks these modifications, we attempted to identify the differences in conformation compared to the fully modified tRNA^{Val}. However, all available structures of full-length *E. coli* tRNA^{Val1} (Rozov et al. 2016; Amiri and Noller 2019; Watson et al. 2020), which were determined in the context of the ribosome-bound complex, are also devoid of modifications. Meanwhile, X-ray crystal structures of the ASL domain of *E. coli* tRNA^{Val1} (ASL^{Val1}) complexed with 30S ribosome (Weixlbaumer et al. 2007)

contain cmo^{5}U34 and m^{6}A37, therefore we used this information to interrogate the structural differences by superposing with the ASL domain of protomer B. When superimposed, two conformations are similar to each other with rmsd of 0.98 ± 0.07 Å, although a noticeable deviation can be observed around the U33–U34 tandem (Fig. 4A). Of note, cmo^{5}U34 forms an additional hydrogen bond via its N3 with the N7 of A35 at ~3.09 Å, presumably as a consequence of altered electrochemical properties of the modified base (Fig. 4B; Weixlbaumer et al. 2007). Moreover, the ribose of wobble uridine is shifted by 2.32 ± 0.02Å in the modified ASL^{Val} in comparison to the unmodified one, where the ribose group of cmo^{5}U34 makes close contact with C1054 of 16S rRNA. These features are likely to contribute to the binding to and unique base-pairing ability of tRNA^{Val} on the ribosome. The structural dissimilarity arising from the N6-methylation of A37 appears to be less obvious in our analyses (Fig. 4C).

Metal-binding sites

High-resolution X-ray diffraction data allowed us to identify six Mg^{2+} and four Na$^+$ in the structure, which are spread over two protomers (Supplemental Figs. 4, 5). Assignment of metal was based on the coordination

TABLE 2. The torsion angle of backbone in the *E. coli* tRNA^{Val1} anticodon stem–loop

Residue		α	β	γ	δ	ε	ζ	χ
32	A	285.0	165.3	68.4	82.9	221.2	285.1	193.2
	B	294.5	169.5	57.9	79.4	222.6	286.2	192.6
33	A	303.2	159.3	57.3	83.9	104.9	298.3	201.8
	B	309.3	164.1	48.3	81.6	227.2	323.6	198.8
34	A	298.2	161.3	195.5	138.2	278.9	208.8	251.7
	B	147.7	134.5	52.7	85.9	251.6	270.7	184.9
35	A	305.5	168.6	44.8	75.2	215.8	319.1	185.3
	B	297.6	147.8	55.6	80.4	217.2	287.8	206.2
36	A	278.9	177.4	57.4	79.5	222.8	304.4	197.5
	B	296.4	167.4	47.4	76.0	213.4	293.0	211.6
37	A	290.9	174.4	54.2	79.0	215.6	296.5	191.7
	B	292.1	176.8	57.3	81.7	215.1	297.9	190.5
38	A	296.9	177.5	52.8	83.4	226.5	299.6	182.2
	B	293.0	170.7	57.5	81.9	216	301.7	186.3

Shown are the torsion angles in degrees (°), which were defined by Hershkovitz et al. (2006).
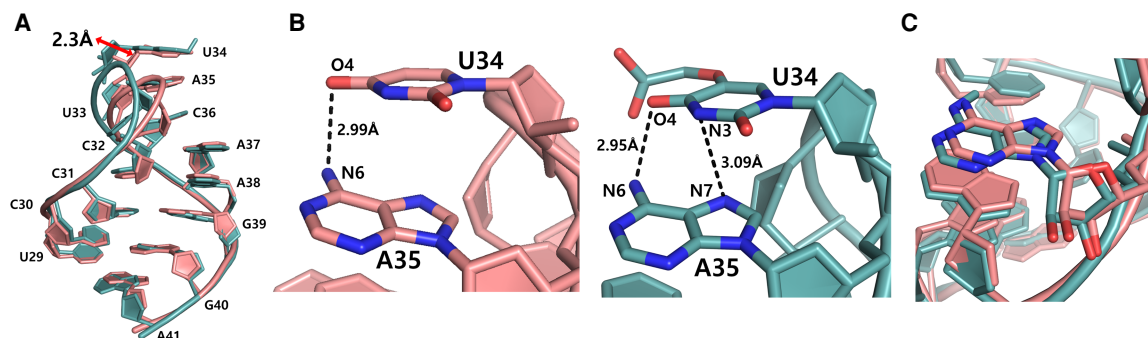
FIGURE 4. Structural comparison of modified and unmodified ASL^{Val1}. Anticodon loops of protomer B (salmon) and modified ASL^{Val} (teal, PDB code: 2UUA) are superposed. (*A*) Comparison of overall tertiary structures, where the phosphate backbone is shown as a tube. The distance between the 2′-OH of wobble uridines is labeled. (*B*) A close-up view of atomic interactions between U34 and A35, where an additional hydrogen bond is made between the N3 of U34 and the N7 of A35 in the modified ASL. Averaged distances of hydrogen bonds are labeled. (*C*) A close-up of A37/m^{6}A37 and neighboring residues.

distance, geometry, and *B*-factor (Leonarski et al. 2017). For example, Mg^{2+} was modeled in electron density near G19 in both protomers, which is coordinated to phosphate oxygen (OP1) and five water molecules in the octahedral metal sphere (Fig. 5A). The distance between the metal and water ranges from 1.86 to 2.18 Å, where that between OP1 and magnesium ion is 2.02 Å. Of interest, Mg^{2+} identified next to G15 is coordinated to the N7 of the nucleobase and five water molecules in both chains, providing a rare example of Mg^{2+} coordination to the nitrogen of nucleic acids (Leonarski et al. 2017). The distance between the metal ion and the N7 of G15 is 2.26 and 2.29 Å in chains A and B, respectively, which is in good agreement with the previously reported values (Wilds et al. 2002; Ohishi et al. 2007). Meanwhile, the distance from this Mg^{2+} to water molecules ranges from 1.91 and 2.29 Å and the overall octahedral coordination geometry is clearly identifiable in the omit density map (Fig. 5B). The fourth magnesium ion is located around the D-arm of chain B (encompassing U8$_B$ through C13$_B$), which is surrounded by six water molecules at an average distance of 2.14 ± 0.08 Å without making direct contact with the nucleic acid. Although a similar electron density feature around the corresponding location in protomer A was observed during the refinement of the model, Na$^+$ was assigned instead considering long distances to the coordinating water molecules (average distance 2.27 ± 0.08 Å). The last magnesium ion is located next to A37$_B$, which is bound to OP1 at 2.24 Å and five water molecules at an average distance of 2.18 ± 0.11 Å. In the equivalent position of protomer A, however, the sodium ion was modeled due to longer distances to ligands (2.61 Å to OP1 and 2.39 ± 0.16 Å to water) and lack of octahedral geometry of the coordination shell, where the metal ion is bound with OP1 of A37$_A$ and four water molecules. The remaining two metal-binding sites were modeled with Na$^+$, which bridges the phosphate groups of G20 and A21 in both protomers. These sodium ions are additionally bound with three water molecules, and the average distance to the coordinating oxygen atoms is 2.43 ± 0.18 Å, too distant for a magnesium ion.

DISCUSSION

The present crystal structure of unbound *E. coli* tRNA^{Val1} displays two different conformational states especially of stacked and flipped-out wobble uridine in the anticodon loop. To our knowledge, the wobble nucleotide is in a stacked conformation in all known structures of free tRNA. Furthermore, crystal structures of tRNA-bound ribosome show that the

FIGURE 5. Representative magnesium-binding sites. An *Fo–Fc* omit electron density map is illustrated as mesh contoured at 3σ. Note the evident octahedral geometry of the coordination shell. Mg^{2+} and water are shown as green and red spheres, respectively. (*A*) Mg^{2+} is coordinated at OP1 of G19 and five water molecules. (*B*) Mg^{2+} is coordinated to the N7 of G15 and five water molecules.

stacking of anticodon triplets of tRNA enables base-pairings with the corresponding codon in the A-site (Ogle et al. 2001). A similar arrangement of anticodon triplets can also be observed in the cocrystal structures of tRNA and the T box riboswitch, where stacked anticodon bases are recognized via base-pairings with a specifier sequence of the riboswitch molecule (Zhang and Ferré-D'Amaré 2013; Battaglia et al. 2019). The base flipping of wobble nucleotide appears to be necessary for modifying enzymes to gain access to the target. However, the destacking of the base would be energetically unfavorable unless compensated by new interactions through protein binding. Notably, the protein-induced rearrangement of the anticodon loop structure results in splaying out of multiple bases within the loop to increase the contact area with the bound protein in those structures (Xie et al. 2003; Hoang et al. 2006; Losey et al. 2006; Byrne et al. 2015). The flipping of U34 in the present structure causes a minimal and localized change in the anticodon loop compared to the previous examples, presumably due to the lack of extensive intermolecular interactions to support such a large restructuring of the loop.

It has been shown that the wobble uridine of tRNA^{Val1} in *E. coli* is targeted for post-transcriptional modifications by multiple enzymes; O$_2$-dependent TrhO or prephenate-dependent TrhP direct the synthesis of 5-hydroxyuridine (ho^{5}U34) (Lauhon 2019; Sakai et al. 2019), which is subsequently modified by carboxymethyl transferase, CmoB, to complete the formation of cmo^{5}U34 (Kim et al. 2013, 2015). Therefore, these enzymes need access to the wobble uridine to carry out the chemical transformation, which would require the destacking of U34. Similarly, equivalent tRNA isoacceptors in *Bacillus subtilis* are subject to 5-methoxyuridine (mo^{5}U34) modification, which requires TrhO, TrhP, and TrmR. TrmR is a homolog of CmoB, which modifies ho^{5}U34 to mo^{5}U34 by methylating the 5-hydroxyl group using SAM as the methyl donor. The cocrystal structure of *B. subtilis* TrmR with unmodified ASL of tRNA^{Ala} was determined recently (Ryu et al. 2018); however, the wobble uridine in the cocrystal structure is stacked on G35 and not optimally positioned to serve as a nucleophile. It was proposed that base-flipping must be proceeded prior to the nucleophilic attack on the *S*-methyl group of SAM, which would have brought the target uracil base closer to the electrophile.

All full-length tRNA^{Val} and ASL^{Val} structures reported to date exhibit stacked conformation of U34 regardless of base modifications or ribosome binding. NMR structures of unbound ASL^{Val} with or without cmo^{5}U34 and m^{6}A37 modifications reveal that the wobble uridine is the most dynamic residue in both unmodified and modified tRNA, reinforcing an inherent dynamic nature of the wobble nucleotide (Vendeix et al. 2008). Of interest, the recently reported X-ray crystal structure of unmodified tRNA^{Asp} demonstrates that U33 is flipped out of the loop and

does not play the conventional role in forming the U-turn motif (Chan et al. 2020). These collective results supporting the plasticity of anticodon loop conformation are in line with our findings, where the flipping of a wobble base could be induced by a small lattice contact in the crystal.

High-resolution diffraction data allowed us to assign a total of 10 metal-binding sites over two NCS-related tRNA molecules, eight of which make direct contact with nucleic acids. Interestingly, Mg^{2+} identified next to G15 is coordinated through the N7 of the guanine base in both protomers. A recent analysis of Mg^{2+} binding to a nucleobase imine nitrogen (N1, N3, and N7) among nucleic acid structures containing magnesium revealed that such cases were extremely rare and could be found in only ~0.5% of the surveyed structures (Leonarski et al. 2017). A similar example showing the Mg^{2+} binding to the imine nitrogen of tRNA is the cocrystal structure of *E. coli* dihydrouridine synthase C (DusC) complexed with tRNA^{Phe} (PDB code 4YCO), where the metal ion contacts the N7 of G15 at approximately 2.3 Å (Byrne et al. 2015). However, as Leonarski et al. pointed out, the distances to water molecules from the metal ion are longer (an average distance of 2.21 Å) than what is expected for Mg^{2+} (2.06 Å), which confers difficulties in clearly distinguishing Mg^{2+} from Na$^+$ (Leonarski et al. 2017). In proteins, magnesium is found to be coordinated to nitrogen atoms in the imidazole ring from histidine side chains. For example, the 2.72 Å crystal structure of spinach light-harvesting complex (PDB code 1RWT) shows that a magnesium ion embedded in the tetrapyrrole ring of chlorophyll is bound to an axially positioned histidine residue at 2.27 ± 0.03 Å (Liu et al. 2004).

MATERIALS AND METHODS

tRNA preparation

The *Escherichia coli* tRNA^{Val} sample was produced from in vitro transcription by T7 RNA polymerase (Milligan et al. 1987; Pleiss et al. 1998). The double-strand DNA templates for tRNA were purchased from IDT (Intergrated DNA Technology) containing T7 promoter in the upstream of the tRNA sequences. The sequences of two templates are as follows: 5′-CTAATACGACTCACTATAGGGTGATTAGCTCAGCTGGGAGAGCACCTCCCTTACAAGGAGGGGGTCGGCGGTTCGATCCCGTCATCACCCACCA-3′ and 5′-TGGTGGGTGATGACGGGATCGAACCGCCGACCCCCTCCTTGTAAGGGAGGTGCTCTCCCAGCTGAGCTAATCACCCTATAGTGAGTCGTATTAG-3′.

DNA templates were purified by 15% urea-acrylamide gel electrophoresis before use. A total of 10 nmoles of DNA templates was used for in vitro transcription with 80 μg/mL T7 RNA polymerase and 2.5 mM rNTP. The transcription mixture was incubated in 37°C in the reaction buffer (40 mM Tris-HCl pH 8.0, 1 mM spermidine, 0.01% [v/v] Triton X-100, 2.5 mM DTT, 25 mM MgCl$_2$) for 6 h. The reaction was terminated by adding 500 μL of 0.5 M

EDTA+. Transcripts were precipitated by adding ethyl with 3 M sodium acetate (pH 5.3) and stored at −20°C. Then, the precipitated RNA pellet was dissolved in DW and purified using urea-acrylamide gel electrophoresis. The eluted RNA from the gel was precipitated by isopropyl alcohol followed by three rounds of washing with 75% (v/v) cold ethyl alcohol. The final pellet was dissolved in DW for further usage.

Crystallization

Initially, we attempted to cocrystallize *Mycoplasma capricolum* YfiC and *E. coli* tRNA^Val. First, 0.08 mM protein and 0.12 mM of tRNA^Val were mixed and incubated at room temperature for 1 h. Protein–tRNA solution was then added to the mixture of 90 mM HEPES (pH 7.5), 45 mM magnesium chloride hexahydrate, 27% (v/v) polyethylene glycol monomethyl ether 550, and 3% (v/v) 2-propanol in 1:1(v/v) ratio. Crystallization was done by the sitting-drop method at room temperature. The crystals appeared after 7 d and were harvested and flash-frozen without the use of cryoprotectant.

X-ray diffraction data collection, structure determination, and refinement

Diffraction data were collected at Beamline PAL 5C in the Pohang Accelerator Laboratory (Pohang, Republic of Korea) using the Dectris Eiger X9M detector at $\lambda = 0.97926$ Å. Collected data were indexed, integrated, and scaled by HKL2000 (Otwinowski and Minor 1997). To solve the phases of structure factors, molecular replacement was performed with Molrep (Vagin and Teplyakov 2010) using tRNA^Val (PDB code 7K00) as a search model. Subsequent model building and refinement were performed iteratively using *Coot* (Emsley et al. 2010), and Phenix Refine (Afonine et al. 2012). Detailed crystallographic statistics are summarized in Table 1.

DATA DEPOSITION

Atomic coordinates and structure factors for crystal structure have been deposited with the Protein Data Bank under accession number 7EQJ.

SUPPLEMENTAL MATERIAL

Supplemental material is available for this article.

ACKNOWLEDGMENTS

REFERENCES

Afonine PV, Grosse-Kunstleve RW, Echols N, Headd JJ, Moriarty NW, Mustyakimov M, Terwilliger TC, Urzhumtsev A, Zwart PH, Adams PD. 2012. Towards automated crystallographic structure refinement with phenix.refine. *Acta Crystallogr Sect D Biol Crystallogr* **68:** 352–367. doi:10.1107/S0907444912001308

Amiri H, Noller HF. 2019. Structural evidence for product stabilization by the ribosomal mRNA helicase. *RNA* **25:** 364–375. doi:10.1261/rna.068965.118

Ashraf SS, Guenther RH, Ansari G, Malkiewicz A, Sochacka E, Agris PF. 2000. Role of modified nucleosides of yeast tRNA^Phe in ribosomal binding. *Cell Biochem Biophys* **33:** 241–252. doi:10.1385/CBB:33:3:241

Auffinger P, Westhof E. 2001. An extended structural signature for the tRNA anticodon loop. *RNA* **7:** 334–341. doi:10.1017/S1355838201002382

Balasubramanian R, Seetharamulu P. 1983. A conformational rationale for the wobble behaviour of the first base of the anticodon triplet in tRNA. *J Theor Biol* **101:** 77–86. doi:10.1016/0022-5193(83)90273-4

Battaglia RA, Grigg JC, Ke A. 2019. Structural basis for tRNA decoding and aminoacylation sensing by T-box riboregulators. *Nat Struct Mol Biol* **26:** 1106–1113. doi:10.1038/s41594-019-0327-6

Begley U, Dyavaiah M, Patil A, Rooney JP, DiRenzo D, Young CM, Conklin DS, Zitomer RS, Begley TJ. 2007. Trm9-catalyzed tRNA modifications link translation to the DNA damage response. *Mol Cell* **28:** 860–870. doi:10.1016/j.molcel.2007.09.021

Boccaletto P, MacHnicka MA, Purta E, Pitkowski P, Baginski B, Wirecki TK, De Crécy-Lagard V, Ross R, Limbach PA, Kotter A, et al. 2018. MODOMICS: a database of RNA modification pathways. 2017 update. *Nucleic Acids Res* **46:** D303–D307. doi:10.1093/nar/gkx1030

Byrne RT, Jenkins HT, Peters DT, Whelan F, Stowell J, Aziz N, Kasatsky P, Rodnina M V, Koonin E V, Konevega AL, et al. 2015. Major reorientation of tRNA substrates defines specificity of dihydrouridine synthases. *Proc Natl Acad Sci* **112:** 6033–6037. doi:10.1073/pnas.1500161112

Chan CW, Badong D, Rajan R, Mondragón A. 2020. Crystal structures of an unmodified bacterial tRNA reveal intrinsic structural flexibility and plasticity as general properties of unbound tRNAs. *RNA* **26:** 278–289. doi:10.1261/rna.073478.119

Chang AT, Nikonowicz EP, Barraud P, Schmitt E, Mechulam Y, Dardel F, Tisné C, Auffinger P, Westhof E, Vendeix FAP, et al. 2012. Solution nuclear magnetic resonance analyses of the anticodon arms of proteinogenic and nonproteinogenic tRNA^Gly. *Biochemistry* **51:** 3662–3674. doi:10.1016/j.str.2013.09.001

Emara MM, Ivanov P, Hickman T, Dawra N, Tisdale S, Kedersha N, Hu GF, Anderson P. 2010. Angiogenin-induced tRNA-derived stress-induced RNAs promote stress-induced stress granule assembly. *J Biol Chem* **285:** 10959–10968. doi:10.1074/jbc.M109.077560

Emsley P, Lohkamp B, Scott WG, Cowtan K. 2010. Features and development of *Coot. Acta Crystallogr Sect D Biol Crystallogr* **66:** 486–501. doi:10.1107/S0907444910007493

Fonvielle M, Chemama M, Villet R, Lecerf M, Bouhss A, Valéry JM, Ethève-Quelquejeu M, Arthur M. 2009. Aminoacyl-tRNA recognition by the FemXWv transferase for bacterial cell wall synthesis. *Nucleic Acids Res* **37:** 1589–1601. doi:10.1093/nar/gkn1039

Hershkovitz E, Sapiro G, Tannenbaum A, Williams LD. 2006. Statistical analysis of RNA backbone. *IEEE/ACM Trans Comput Biol Bioinform* **3:** 33–46. doi:10.1109/TCBB.2006.13

Hoang C, Chen J, Vizthum CA, Kandel JM, Hamilton CS, Mueller EG, Ferré-D'Amaré AR. 2006. Crystal structure of pseudouridine synthase RluA: indirect sequence readout through protein-induced

RNA structure. *Mol Cell* **24:** 535–545. doi:10.1016/j.molcel.2006.09.017

Ivanov P, Emara MM, Villen J, Gygi SP, Anderson P. 2011. Angiogenin-induced tRNA fragments inhibit translation initiation. *Mol Cell* **43:** 613–623. doi:10.1016/j.molcel.2011.06.022

Kim SH, Suddath FL, Quigley GJ, McPherson A, Sussman JL, Wang AHJ, Seeman NC, Rich A. 1974. Three-dimensional tertiary structure of yeast phenylalanine transfer RNA. *Science* **185:** 435–440. doi:10.1126/science.185.4149.435

Kim J, Xiao H, Bonanno JB, Kalyanaraman C, Brown S, Tang X, Al-Obaidi NF, Patskovsky Y, Babbitt PC, Jacobson MP, et al. 2013. Structure-guided discovery of the metabolite carboxy-SAM that modulates tRNA function. *Nature* **498:** 123–126. doi:10.1038/nature12180

Kim J, Xiao H, Koh J, Wang Y, Bonanno JB, Thomas K, Babbitt PC, Brown S, Lee YS, Almo SC. 2015. Determinants of the CmoB carboxymethyl transferase utilized for selective tRNA wobble modification. *Nucleic Acids Res* **43:** 4602–4613. doi:10.1093/nar/gkv206

Kurata S, Weixlbaumer A, Ohtsuki T, Shimazaki T, Wada T, Kirino Y, Takai K, Watanabe K, Ramakrishnan V, Suzuki T. 2008. Modified uridines with C5-methylene substituents at the first position of the tRNA anticodon stabilize U·G wobble pairing during decoding. *J Biol Chem* **283:** 18801–18811. doi:10.1074/jbc.M800233200

Lauhon CT. 2019. Identification and characterization of genes required for 5-hydroxyuridine synthesis in *Bacillus subtilis* and *Escherichia coli* tRNA. *J Bacteriol* **201:** e00433-19. doi:10.1128/JB.00433-19

Lee SR, Collins K. 2005. Starvation-induced cleavage of the tRNA anticodon loop in *Tetrahymena thermophila*. *J Biol Chem* **280:** 42744–42749. doi:10.1074/jbc.M510356200

Lennarz WJ, Nesbitt JA, Reiss J. 1966. The participation of sRNA in the enzymatic synthesis of O-L-lysyl phosphatidylgylcerol in *Staphylococcus aureus*. *Proc Natl Acad Sci* **55:** 934–941. doi:10.1073/pnas.55.4.934

Leonarski F, D'Ascenzo L, Auffinger P. 2017. Mg²⁺ ions: do they bind to nucleobase nitrogens? *Nucleic Acids Res* **45:** 987–1004. doi:10.1093/nar/gkw1175

Li S, Su Z, Lehmann J, Stamatopoulou V, Giarimoglou N, Henderson FE, Fan L, Pintilie GD, Zhang K, Chen M, et al. 2019. Structural basis of amino acid surveillance by higher-order tRNA-mRNA interactions. *Nat Struct Mol Biol* **26:** 1094–1105. doi:10.1038/s41594-019-0326-7

Liu Z, Yan H, Wang K, Kuang T, Zhang J, Gui L, An X, Chang W. 2004. Crystal structure of spinach major light-harvesting complex at 2.72 Å resolution. *Nature* **428:** 287–292. doi:10.1038/nature02373

Losey HC, Ruthenburg AJ, Verdine GL. 2006. Crystal structure of *Staphylococcus aureus* tRNA adenosine deaminase TadA in complex with RNA. *Nat Struct Mol Biol* **13:** 153–159. doi:10.1038/nsmb1047

Mei Y, Yong J, Liu H, Shi Y, Meinkoth J, Dreyfuss G, Yang X. 2010. tRNA binds to cytochrome *c* and inhibits caspase activation. *Mol Cell* **37:** 668–678. doi:10.1016/j.molcel.2010.01.023

Milligan JF, Groebe DR, Witherell GW, Uhlenbeck OC. 1987. Oligoribonucleotide synthesis using T7 RNA polymerase and synthetic DNA templates. *Nucleic Acids Res* **15:** 8783–8798. doi:10.1093/nar/15.21.8783

Ogle JM, Brodersen DE, Clemons J, Tarry MJ, Carter AP, Ramakrishnan V. 2001. Recognition of cognate transfer RNA by the 30S ribosomal subunit. *Science* **292:** 897–902. doi:10.1126/science.1060612

Ohishi H, Tozuka Y, Da-Yang Z, Ishida T, Nakatani K. 2007. The rare crystallographic structure of d(CGCGCG)$_2$: the natural spermidine molecule bound to the minor groove of left-handed Z-DNA d (CGCGCG)$_2$ at 10°C. *Biochem Biophys Res Commun* **358:** 24–28. doi:10.1016/j.bbrc.2007.04.026

Otwinowski Z, Minor W. 1997. Processing of X-ray diffraction data collected in oscillation mode. *Methods Enzymol* **276:** 307–326. doi:10.1016/S0076-6879(97)76066-X

Phelps SS, Malkiewicz A, Agris PF, Joseph S. 2004. Modified nucleotides in tRNA^{Lys} and tRNA^{Val} are important for translocation. *J Mol Biol* **338:** 439–444. doi:10.1016/j.jmb.2004.02.070

Pleiss JA, Derrick ML, Uhlenbeck OC. 1998. T7 RNA polymerase produces 5′ end heterogeneity during in vitro transcription from certain templates. *RNA* **4:** 1313–1317. doi:10.1017/S13558382 9800106X

Quigley GJ, Rich A. 1976. Structural domains of transfer RNA molecules. *Science* **194:** 796–806. doi:10.1126/science.790568

Ranjan N, Rodnina MV. 2017. Thio-modification of tRNA at the wobble position as regulator of the kinetics of decoding and translocation on the ribosome. *J Am Chem Soc* **139:** 5857–5864. doi:10.1021/jacs.7b00727

Robertus JD, Ladner JE, Finch JT, Rhodes D, Brown RS, Clark BFC, Klug A. 1974. Structure of yeast phenylalanine tRNA at 3 Å resolution. *Nature* **250:** 546–551. doi:10.1038/250546a0

Rould MA, Perona JJ, Steitz TA. 1991. Structural basis of anticodon loop recognition by glutaminyl-tRNA synthetase. *Nature* **352:** 213–218. doi:10.1038/352213a0

Roy H, Ibba M. 2009. Broad range amino acid specificity of RNA-dependent lipid remodeling by multiple peptide resistance factors. *J Biol Chem* **284:** 29677–29683. doi:10.1074/jbc.M109.046367

Rozov A, Westhof E, Yusupov M, Yusupova G. 2016. The ribosome prohibits the G•U wobble geometry at the first position of the codon-anticodon helix. *Nucleic Acids Res* **44:** 6434–6441. doi:10.1093/nar/gkw431

Ryu H, Grove TL, Almo SC, Kim J. 2018. Identification of a novel tRNA wobble uridine modifying activity in the biosynthesis of 5-methoxyuridine. *Nucleic Acids Res* **46:** 9160–9169. doi:10.1093/nar/gky592

Sakai Y, Kimura S, Suzuki T. 2019. Dual pathways of tRNA hydroxylation ensure efficient translation by expanding decoding capability. *Nat Commun* **10:** 2858. doi:10.1038/s41467-019-10750-8

Salman Ashraf S, Sochacka E, Cain R, Guenther R, Malkiewicz A, Agris PF. 1999. Single atom modification (O→S) of tRNA confers ribosome binding. *RNA* **5:** 188–194. doi:10.1017/S13558382 99981529

Thompson DM, Parker R. 2009. Stressing out over tRNA cleavage. *Cell* **138:** 215–219. doi:10.1016/j.cell.2009.07.001

Thompson DM, Lu C, Green PJ, Parker R. 2008. tRNA cleavage is a conserved response to oxidative stress in eukaryotes. *RNA* **14:** 2095–2103. doi:10.1261/rna.1232808

Urbonavičius J, Qian Q, Durand JMB, Hagervall TG, Björk GR. 2001. Improvement of reading frame maintenance is a common function for several tRNA modifications. *EMBO J* **20:** 4863–4873. doi:10.1093/emboj/20.17.4863

Vagin A, Teplyakov A. 2010. Molecular replacement with MOLREP. *Acta Crystallogr Sect D Biol Crystallogr* **66:** 22–25. doi:10.1107/S0907444909042589

Vendeix FAP, Dziergowska A, Gustilo EM, Graham WD, Sproat B, Malkiewicz A, Agris PF. 2008. Anticodon domain modifications contribute order to tRNA for ribosome-mediated codon binding. *Biochemistry* **47:** 6117–6129. doi:10.1021/bi702356j

Wang Q, Lee I, Ren J, Ajay SS, Lee YS, Bao X. 2013. Identification and functional characterization of tRNA-derived RNA fragments (tRFs) in respiratory syncytial virus infection. *Mol Ther* **21:** 368–379. doi:10.1038/mt.2012.237

Watson ZL, Ward FR, Méheust R, Ad O, Schepartz A, Banfield JF, Cate JHD. 2020. Structure of the bacterial ribosome at 2 Å resolution. *Elife* **9:** e60482. doi:10.7554/eLife.60482

Weixlbaumer A, Murphy FV IV, Dziergowska A, Malkiewicz A, Vendeix FAP, Agris PF, Ramakrishnan V. 2007. Mechanism for expanding the decoding capacity of transfer RNAs by modification of uridines. *Nat Struct Mol Biol* **14:** 498–502. doi:10.1038/nsmb1242

Wilds CJ, Pattanayek R, Pan C, Wawrzak Z, Egli M. 2002. Selenium-assisted nucleic acid crystallography: use of phosphoroselenoates for MAD phasing of a DNA structure. *J Am Chem Soc* **124:** 14910–14916. doi:10.1021/ja021058b

Xie W, Liu X, Huang RH. 2003. Chemical trapping and crystal structure of a catalytic tRNA guanine transglycosylase covalent intermediate. *Nat Struct Biol* **10:** 781–788. doi:10.1038/nsb976

Yarian C, Townsend H, Czestkowski W, Sochacka E, Malkiewicz AJ, Guenther R, Miskiewicz A, Agris PF. 2002. Accurate translation of the genetic code depends on tRNA modified nucleosides. *J Biol Chem* **277:** 16391–16395. doi:10.1074/jbc.M200253200

Zhang J, Ferré-D'Amaré AR. 2013. Co-crystal structure of a T-box riboswitch stem i domain in complex with its cognate tRNA. *Nature* **500:** 363–366. doi:10.1038/nature12440

Zhang J, Ferré-D'Amaré AR. 2015. Structure and mechanism of the T-box riboswitches. *Wiley Interdiscip Rev RNA* **6:** 419–433. doi:10.1002/wrna.1285